

Reconstruction and forecasting of slow-moving landslide displacement using a Kalman Filter approach

Mohit Mishra¹, Gildas Besançon¹, Guillaume Chambon², and Laurent Baillet³

¹Univ. Grenoble Alpes, CNRS, Grenoble INP - Institute of Engineering, GIPSA-Lab, 38000, Grenoble, France

²Univ. Grenoble Alpes, CNRS INRAE, IRD, Grenoble INP - Institute of Engineering, IGE, Grenoble, France

³Univ. Grenoble Alpes, CNRS, ISTERre, Grenoble, France

Correspondence: Gildas Besançon (gildas.besancon@grenoble-inp.fr)

Abstract. This work presents an approach for reconstructing displacement evolution and unknown soil properties of slow-moving landslides, using a special form of so-called *Kalman filter* or *observer*. The approach relies on a mechanical model for the prediction step, with online correction based on available measurements. The observer proposed here relies on a simplified 1D viscoplastic sliding model. Landslide (slide block) motion is controlled by a balance between gravity and sliding resistance expressed in terms of friction, basal pore fluid pressure, cohesion, and viscosity. In order to improve the observer performance upon abrupt changes in parameters, a resetting method is proposed. A novel tuning algorithm, based on a combination of synthetic and actual test cases, is introduced to overcome the sensitivity to observer coefficients. Known parameter values (landslide geometrical parameters and known material properties) as well as water-table height time series are provided as inputs. The observer then reconstructs landslide displacement and the evolution of unknown parameters over time. The case of Super-Sauze landslide (French Alps), with data taken from the literature, is used to illustrate the potential of the approach. Finally, the observer is extended to forecast displacement evolution over different temporal horizons assuming that future water-table height variations are known.

1 Introduction

Landslides can have severe consequences in terms of fatalities and injuries as well as of damages to infrastructures and ecosystems (Froude and Petley, 2018; Petley, 2012; Kjekstad and Highland, 2009). The capacity to detect and forecast such disasters in advance through Early Warning Systems (EWS) is critical to take timely corrective measures and reduce economic and life losses (Guzzetti et al., 2020; Pecoraro et al., 2019). In this context, combination of landslide monitoring and modelling techniques can help determining the stability of the slopes and identifying landslide triggering factors, with the objective of predicting ground movements (Pradhan et al., 2019; Bernardie et al., 2014; Springman et al., 2013; Herrera et al., 2013; Corominas et al., 2005).

Monitoring slopes provides critical information on kinematic, hydrological, and meteorological parameters. A large variety of instruments and geophysical methods can be used, e.g., Global Positioning System (GPS), photogrammetry, remote sensing (LiDAR, InSAR, etc.), Electrical Resistivity Tomography (ERT), Ground Penetrating Radar (GPR), geotechnical techniques (inclinometers, piezometers, extensometer, Radio Frequency Identification (RFID), Shape Acceleration Arrays (SAA), etc.

25 (Casagli et al., 2023; Pecoraro et al., 2019; Breton et al., 2019; Bottelin et al., 2017; Larose et al., 2015; Angeli et al., 2000; Gili et al., 2000). The most commonly measured parameters are ground displacement, groundwater pressure head and rainfall.

These parameters can then be used to develop and inform landslide mobility models for forecasting purposes. Broadly-speaking, two main categories of models can be utilized to predict landslide mobility. Phenomenological models are based on empirical relationships (Guzzetti et al., 2008; Larsen and Simon, 1993; Caine, 1980), statistical approaches (Capparelli and
30 Versace, 2011; Capparelli and Tiranti, 2010), or artificial neural networks (Kumar et al., 2021; Bui et al., 2020; Yang et al., 2019; Mayoraz and Vulliet, 2002), to establish relations between soil displacement and landslide-inducing factors, e.g., rainfall or water table fluctuations. However, as these models generally lack temporal aspects, they are unable to account for changes in landslide-controlling conditions (Westen, 2004). Alternatively, mechanics-based models rely on deterministic laws to represent the physical processes controlling landslide occurrence and dynamics (Dikshit et al., 2019; Kim et al., 2016; Pradhan and Kim,
35 2014; Teixeira et al., 2014; Alvioli et al., 2014; Ali et al., 2014; Herrera et al., 2013; Van Asch et al., 2007; Corominas et al., 2005; Angeli et al., 1998; Asch and Genuchten, 1990; Hutchinson, 1986). Some combined statistical-mechanical models have also been developed for the investigation of landslide displacement, pore water pressure, and rainfall (e.g. Bernardie et al., 2014).

It can be noticed that physically-based landslide models are sensitive to initial conditions as well as to a number of parameters
40 (related to geometrical and geotechnical properties) that can be constant or time-varying. Some of these parameters can be inferred from field observations, laboratory, and in situ tests, while others need to be estimated through inversion techniques. The most frequently used approach to estimate unknown parameters is by minimizing the difference between measured displacement and displacement computed by the model. Several optimization schemes have been employed in past studies, such as sequential quadratic programming (SQP) (Bernardie et al., 2014) and non-linear regression (Herrera et al., 2013;
45 Corominas et al., 2005). Both methods are adapted for the optimization of non-linear dynamical systems, which can result in sub-optimal solutions, i.e., different sets of estimated parameters depending on optimization initiation. Besides optimization methods (deterministic approach), probabilistic back analysis can also be used (Zuo et al., 2020). Once the unknown parameters are estimated, the model equation can then be solved to forecast displacement patterns (Bernardie et al., 2014).

To summarize, the sensitivity to initial conditions and parameters is generally handled by simulating a model iteratively and
50 adjusting the parameter values to obtain consistency with measured data (iterative approach). Alternatively, another efficient approach can be to run a model over time and continually fine-tune the parameters to synchronize with measured data, as in the so-called *Kalman filter* (or ‘observer’) approach (Kalman, 1960) (continuous approach). This second approach is much less common in landslide studies (see e.g. Lu and Zeng, 2020; Acar et al., 2008) and has seldom be used in conjunction with a mechanics-based model. In former studies, we applied both of these approaches to a landslide sliding consolidation
55 model, using synthetically generated data: see (Mishra et al., 2020a) for the iterative scheme (adjoint method), and (Mishra et al., 2020b) for the continuous scheme (observer design). We found that a continuous scheme can be more suitable for reconstructing time-varying parameters. In addition, Kalman approach has the advantage of providing an *optimal* filtering solution whenever the model is linear and subject to additive white noises (Anderson and Moore, 1979). When used with a

physical model, it shows powerful prediction capabilities thanks to the feedback connection with real data. Lastly, it also offers tuning parameters to act on the filtering / reconstruction performances.

The present paper proposes to investigate further the use of a Kalman approach combined to a mechanical model for landslide monitoring, focusing on the problem of reconstruction of displacement patterns jointly with unknown parameters. As in our previous studies, a simple sliding block model with a limited number of parameters is considered for the sake of illustration. Notice that as a counterpart of the tuning possibilities offered by the Kalman approach, selecting appropriate tuning coefficient may actually prove difficult. In addition, it is known that Kalman approach can be hindered in the presence of nonlinearities in the model, which is a priori the case for the model considered here. Finally, one may have to face unexpected issues when moving from a methodological approach to its actual implementation with real data. In this context, the main contributions of this work are the following: (1) Regarding the model, it is first shown how a linear representation can be derived from the original nonlinear formulation, making the problem amenable to a Kalman approach. (2) Regarding the tuning, the use of an exponential forgetting factor is proposed in the chosen discrete-time observer approach (Ticlea and Besançon, 2013, 2009) to improve reconstruction performances. An original resetting method is introduced in the observer for a better convergence of the estimates. Furthermore, a novel iterative approach for tuning observer coefficients is proposed, considering both real and synthetic test cases. (3) Finally, regarding implementation, it should be emphasized that this study is based on monitoring data (displacement and water table height) measured on a real landslide (Bernardie et al., 2014), and that promising applications to landslide forecasting are also demonstrated.

Since the main objective of this paper is to present the methodology and illustrate its potential on real data, the work relies - as in our previous studies - on a simplified physically-based landslide model depicting block sliding behavior with a predefined slip surface. A viscoplastic sliding resistance law is assumed (Herrera et al., 2013). Although extremely simplified, such a 1D approach can provide a first approximation of landslide motion. The targeted applications concern slow-moving landslides whose dynamics is primarily controlled by water table fluctuations. In addition, we assume that water table height is known, and focus on the reconstruction of landslide displacement and mechanical parameters at a single location. Extension of the approach to fully coupled hydromechanical models and/or more complex 2D or 3D mobility models (Chae et al., 2017) shall be considered in future work, but will require more extensive spatial datasets for estimation and prediction purposes.

The structure of the paper is as follows: The simplified viscoplastic sliding model is introduced in Section 2, together with the corresponding estimation problem. Section 3 presents the proposed reconstruction scheme. In Section 4, simulation results illustrate the effectiveness of the estimation scheme on the considered test case, namely Super-Sauze landslide (French Alps). Section 5 extends the proposed observer to the purpose of landslide displacement forecasting, assuming that future water table height variations are known. Finally, Section 6 provides a conclusion and discusses future directions of the work.

2 Simplified landslide viscoplastic sliding model

The viscoplastic sliding model (Bernardie et al., 2014; Herrera et al., 2013; Corominas et al., 2005) represents the dynamics of the landslide as that of a rigid sliding block overlying a thin shear zone, as shown in Fig. 1. The motion is controlled by

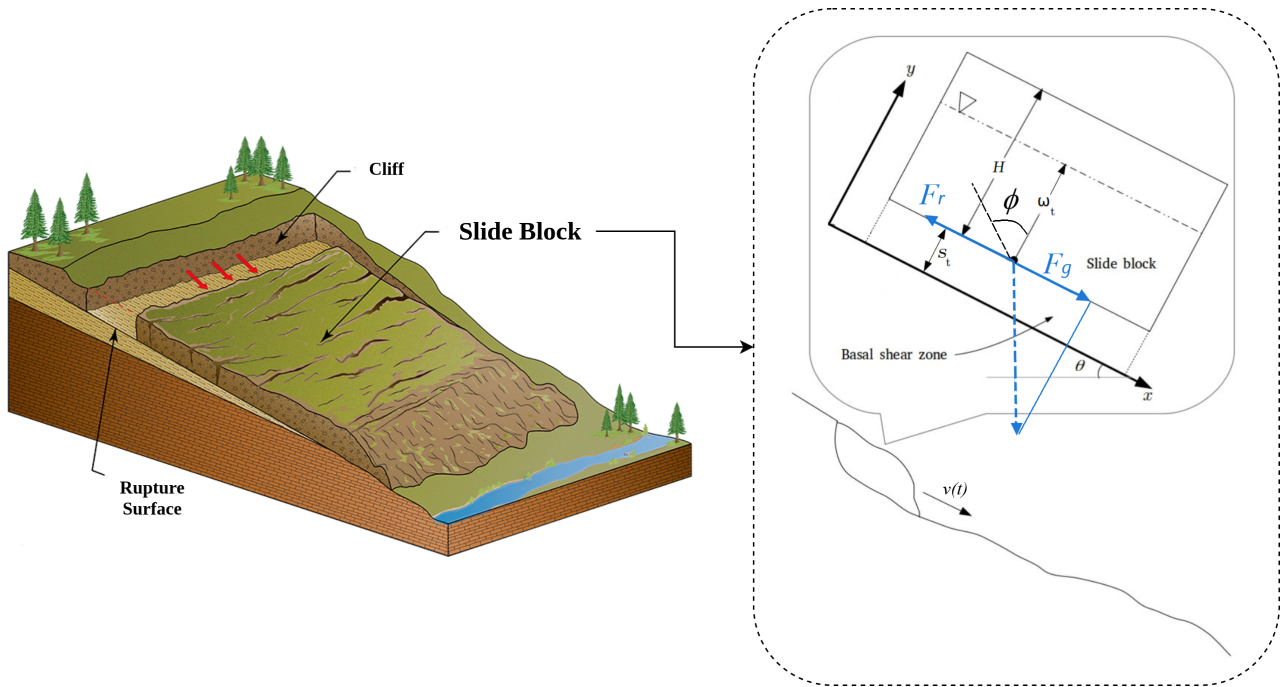


Figure 1. Schematic representation illustrating geometrical and mechanical variables used to model slide block motion: F_r resisting force; F_g driving gravity force; H block height; w_t water table height; s_t shear zone thickness; ϕ friction angle; θ inclination angle; v velocity [left picture is taken from Wyoming State Geological Survey website <https://main.wsgs.wyo.gov/hazards/landslides/types-of-landslides/translational>, Credit: Wyoming State Geological Survey]

difference between the driving force F_g due to gravity and resisting forces F_r due to effective friction, cohesion, and viscosity. Hence, net acceleration of the block a is given by

$$\rho H a(t) = \rho g H \sin \theta - [\rho g H \cos \theta \tan \phi - p(t) \tan \phi + C + \eta v(t) / s_t] \quad (1)$$

95 where ρ is the soil density, H is the slide block height, g is the acceleration due to gravity, θ is the inclination angle, $p(t)$ is the basal pore water pressure at time t , $v(t)$ is velocity of the slide block, and s_t is the basal shear zone thickness. The three mechanical parameters ϕ , C and η denote the friction angle, the cohesion, and the viscosity of the shear zone material, respectively.

For slow-moving landslides, the inertia is expected to remain much smaller than the other terms in Eq. (1), namely $\rho H a \approx 0$.
100 Assuming also that groundwater flow is parallel to the slope surface, the pore water pressure can be expressed as (Bernardie et al., 2014; Iverson, 2000)

$$p(t) = \rho_w g \cos^2 \theta w_t(t) \quad (2)$$

where ρ_w is the pore water density and $w_t(t)$ is water table height, as shown in Fig. 1. Therefore, Eq. (1) can be rewritten as

$$\dot{d} = v(t) = \frac{s_t}{\eta} [\rho H g \sin \theta - \rho \tan \phi H g \cos \theta - C + \rho_w \tan \phi g \cos^2 \theta w_t(t)] \quad (3)$$

105 where d is the displacement of the slide block.

As upslope motion of the rigid slide block is physically impossible, the landslide velocity can not be negative. Such a situation arises whenever water table height $w_t(t)$ goes below a critical water table height w_t^{crit} . From Eq. (3) the value of w_t^{crit} is given by

$$w_t^{crit} = \frac{C - \rho H g \sin \theta + \rho H g \cos \theta \tan \phi}{\rho_w g \cos^2 \theta \tan \phi}. \quad (4)$$

110 When $w_t(t) \leq w_t^{crit}$, landslide dynamics thus reduces to $\dot{d} = v(t) = 0$.

For known parameter values and water-table height (or pore water pressure), time series of displacement can be computed using Eq. (3) for $w_t > w_t^{crit}$ and the above reduced dynamics otherwise. However, some material properties of the landslide (notably friction angle, cohesion and viscosity) are generally unknown, and therefore need to be estimated. In this paper, an observer-based approach is proposed to estimate friction angle ϕ , and viscosity η from measured displacement $d_{mea}(t)$ and

115 water table height $w_t(t)$ time series, assuming cohesion C is known.

3 Reconstruction scheme

3.1 Observer-oriented representation

To address the observer problem, let us first normalize the unknown parameter η by introducing a typical viscosity scale $\bar{\eta}$ in Eq. (3) as follows:

$$120 \quad \bar{\eta} \dot{d} = \left(\frac{\bar{\eta}}{\eta} \right) s_t \rho H g \sin \theta - \left(\frac{\bar{\eta} \tan \phi}{\eta} \right) s_t \rho H g \cos \theta - \left(\frac{\bar{\eta}}{\eta} \right) s_t C + \left(\frac{\bar{\eta} \tan \phi}{\eta} \right) s_t \rho_w g \cos^2 \theta w_t(t). \quad (5)$$

This normalization is introduced to bring all parameters of interest in the same order of magnitude, as friction angle ϕ is dimensionless and usually comprised between 0 and 1.

Further, $\eta/\bar{\eta}$ and ϕ being now the parameters to be estimated, let us define:

$$\begin{bmatrix} \theta_1 \\ \theta_2 \end{bmatrix} := s_t \begin{bmatrix} \rho H g \sin \theta - C & -\rho H g \cos \theta \\ 0 & \rho_w g \cos^2 \theta \end{bmatrix} \begin{bmatrix} \bar{\eta}/\eta \\ \bar{\eta} \tan \phi / \eta \end{bmatrix}. \quad (6)$$

125 This substitution linearizes the model equation, making it more suitable for observer design. In order to estimate parameters, and assuming that those parameters vary slowly, the model can be extended by two additional differential equations, namely $\dot{\theta}_1 = 0, \dot{\theta}_2 = 0$. Substituting Eq. (6) into (5), and taking the expression of w_t^{crit} into account, the system equations finally become:

$$\dot{d} = \begin{cases} \frac{\theta_1}{\bar{\eta}} + \frac{\theta_2}{\bar{\eta}} w_t(t) & \text{if } w_t(t) > w_t^{crit} \\ 0 & \text{otherwise} \end{cases}$$

$$\dot{\theta}_1 = 0, \quad \dot{\theta}_2 = 0. \quad (7)$$

Instruments used for landslide monitoring collect data with a particular time resolution, e.g., hourly. Therefore, to adapt with discrete measurements (at times denoted by t^k), let us express the system dynamics in discrete time as follows

$$\underbrace{\begin{bmatrix} d^{k+1} \\ \theta_1^{k+1} \\ \theta_2^{k+1} \end{bmatrix}}_{x^{k+1}} = \begin{cases} \underbrace{\begin{bmatrix} 1 & \frac{dt}{\eta} & \frac{dt}{\eta} w_t^k \\ 0 & 1 & 0 \\ 0 & 0 & 1 \end{bmatrix}}_{\bar{A}_1^k} \underbrace{\begin{bmatrix} d^k \\ \theta_1^k \\ \theta_2^k \end{bmatrix}}_{x^k}, & \text{if } w_t^k > w_t^{crit} \\ \underbrace{\begin{bmatrix} 1 & 0 & 0 \\ 0 & 1 & 0 \\ 0 & 0 & 1 \end{bmatrix}}_{\bar{A}_2^k} \underbrace{\begin{bmatrix} d^k \\ \theta_1^k \\ \theta_2^k \end{bmatrix}}_{x^k} & \text{otherwise} \end{cases} \quad (8)$$

where $dt = t^{k+1} - t^k$ is the discrete-time step, and x^k gathers all system variables. The measurement model is given as

$$135 \quad y^k = d_{mea}^k = \underbrace{\begin{bmatrix} 1 & 0 & 0 \end{bmatrix}}_{\bar{C}} \underbrace{\begin{bmatrix} d^k \\ \theta_1^k \\ \theta_2^k \end{bmatrix}}_{x^k} + r^k \quad (9)$$

where y^k denotes the actually available measurement, and r^k some measurement noise.

3.3 Discrete-time exponential forgetting factor observer

Discrete-time exponential forgetting factor observer (or Kalman filtering with forgetting factor) provides least mean-square estimate with an added feature of giving more weight to the most recent measurements. If γ denotes the forgetting factor and

140 \hat{x}_0 denotes the initial guess for x^k , the approach optimizes the following objective function:

$$J_k(\hat{x}_0^k) = \gamma^k (\hat{x}_0^k - \hat{x}_0)^T P_0^{-1} (\hat{x}_0^k - \hat{x}_0) + \sum_{l=0}^k \gamma^{k-l} (\hat{y}^l - y^l)^T W^{-1} (\hat{y}^l - y^l) \quad (10)$$

subject to system dynamics

$$\begin{aligned} \hat{x}^{k+1} &= \bar{A}^k \hat{x}^k \\ \hat{y}^k &= \bar{C} \hat{x}^k \end{aligned} \quad (11)$$

as constraints, with $\gamma \in (0, 1)$, $P_0 = P_0^T > 0$, $W = W^T > 0$. The solution of this optimization problem (Țiclea and Besançon,

145 2013) is provided through measurement update equations:

$$\hat{x}_c^k = \hat{x}_p^k - K^k (\bar{C} \hat{x}_p^k - y^k), \quad (12)$$

with

$$K^k = P^k \bar{C}^\top (\bar{C} P_p^k \bar{C}^\top + W)^{-1}, \quad (13)$$

and time update equations,

$$150 \quad \hat{x}_p^{k+1} = \bar{A}^k \hat{x}_c^k \quad (14)$$

$$P^{k+1} = \gamma^{-1} \bar{A}^k [I - K^k \bar{C}] P^k \bar{A}^{k\top} + Q \quad (15)$$

with initialization P_0 . Here K^k is the Kalman gain, P is the auto-covariance of state estimation error, W is the auto-covariance of measurement noise r , $\gamma \in (0, 1)$ is the forgetting factor, and Q is the process noise auto-covariance matrix.

155 For dynamics (8)-(9), observer (12)-(15) provides estimates of \hat{d} , $\hat{\theta}_1$ and $\hat{\theta}_2$. Based on these estimates at each time step, firstly $\bar{\eta}/\hat{\eta}$ and $\bar{\eta} \tan \hat{\phi}/\hat{\eta}$ are reconstructed using Eq. (6):

$$\begin{bmatrix} \bar{\eta}/\hat{\eta} \\ \bar{\eta} \tan \hat{\phi}/\hat{\eta} \end{bmatrix} = \frac{1}{s_t} \begin{bmatrix} \rho H g \sin \theta - C & -\rho H g \cos \theta \\ 0 & \rho_w g \cos^2 \theta \end{bmatrix}^{-1} \begin{bmatrix} \hat{\theta}_1 \\ \hat{\theta}_2 \end{bmatrix}, \quad (16)$$

followed by

$$\hat{\eta} = \frac{\bar{\eta}}{[\bar{\eta}/\hat{\eta}]} \quad \& \quad \hat{\phi} = \tan^{-1} \left(\left[\bar{\eta} \tan \hat{\phi}/\hat{\eta} \right] \frac{\hat{\eta}}{\bar{\eta}} \right). \quad (17)$$

160 In the proposed estimation scheme, w_t^{crit} plays an important role. This quantity itself depends on the parameter values, therefore at each step it is estimated using Eq. (4).

3.4 State estimation error covariance matrix P resetting

In the design presented so far, unknown parameters are assumed to be constant or slowly varying. However, in practical applications, these parameters may also be subject to abrupt changes. In order to handle such situations, a resetting of state estimation error covariance matrix P is proposed here. In order to detect abrupt variations, the Mahalanobis distance (Gnanadesikan and Kettenring, 1972) between actual and predicted measurements for some previous times (t^{k-m} to t^k), with more weight on the most recent times, is calculated as:

$$D^k = \sum_{j=k-m}^k \gamma^{k-j} (C^j \hat{x}^j - y^j)^T W^{-1} (C^j \hat{x}^j - y^j). \quad (18)$$

At times for which D^k exceeds a given threshold ($D^k > \chi^2$), P^k is reset to P_0 . This threshold can be obtained from the *chi-square* table (Pearson, 1900) according to the confidence level of the measurement system. For example, when confidence level is 99% and the dimension of the measurement system vector is 1, the corresponding *chi-square* value is $\chi^2 = 6.635$. Note that there is a possibility of multiple successive resettings, which could hamper the overall performance of the estimation scheme. Such a scenario is avoided by forbidding resetting for some short duration (e.g., m instances) after each detected resetting.

3.5 Observer coefficients tuning

175 Observer coefficients $(P_0, W, Q, \gamma, \chi^2, m)$ should be properly chosen to recover model information (see Fig. 2). In usual applications, these coefficients are manually tuned until proper convergence in estimates are obtained. However, such applications require some nominal values of the parameters being known (e.g. Țiclea and Besançon, 2009), which is not the case in the present study. Therefore, a novel approach is introduced, which considers both synthetic and actual data cases to verify the estimates, according to the methodology summarized in Fig. 3.

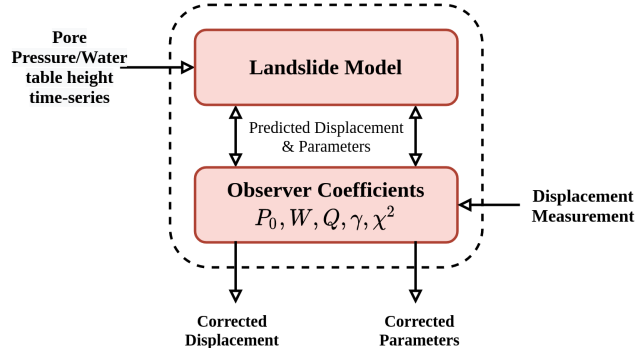


Figure 2. Principle of discrete-time exponential forgetting factor observer.

180 In this approach, given an assumed confidence level in the measurement model and a known dimension of the measurement vector, the value of χ^2 is fixed throughout the tuning process. Along with χ^2 , P_0 and m are also fixed. The matrix P_0 is obtained from its definition with guessed initial states \hat{x}_0 . The coefficient m is guessed from some rough initial simulation results on synthetic test cases and can be chosen from the time steps required for first convergence. Once filter coefficients χ^2 , P_0 and m are fixed, the estimation scheme is applied on real measurements with some initial values of Q , γ and W . For the actual data
185 case, W is manually tuned until $W \approx W_m$ where, W_m is the variance of signal $d_{mea} - \hat{d}$. Then synthetic measurements are generated by solving Eq. (3) using water table height measurements and estimated parameters (smoothed estimated viscosity and averaged estimated frictional angle) from an actual data case. Now estimation scheme is employed on these synthetic measurements keeping filter coefficients W , γ , and Q identical as in the actual case. If estimated parameters from both actual
190 of quantitative indicator I_q given as

$$I_q = \sum_{k=1}^n \left| \frac{q^k - \hat{q}^k}{q^k} \right| \quad (19)$$

where q^k is the parameter of interest (viscosity and friction angle) at time k and \hat{q}^k is the corresponding estimated parameter. Indicator I_q provides information on how close the estimated parameters are to the parameters used to generate the synthetic test case. The above process of tuning W from actual case, followed by tuning γ and Q on synthetic test cases, is continued
195 until parameter estimates in both cases are consistent to each other, as shown in Fig. 3.

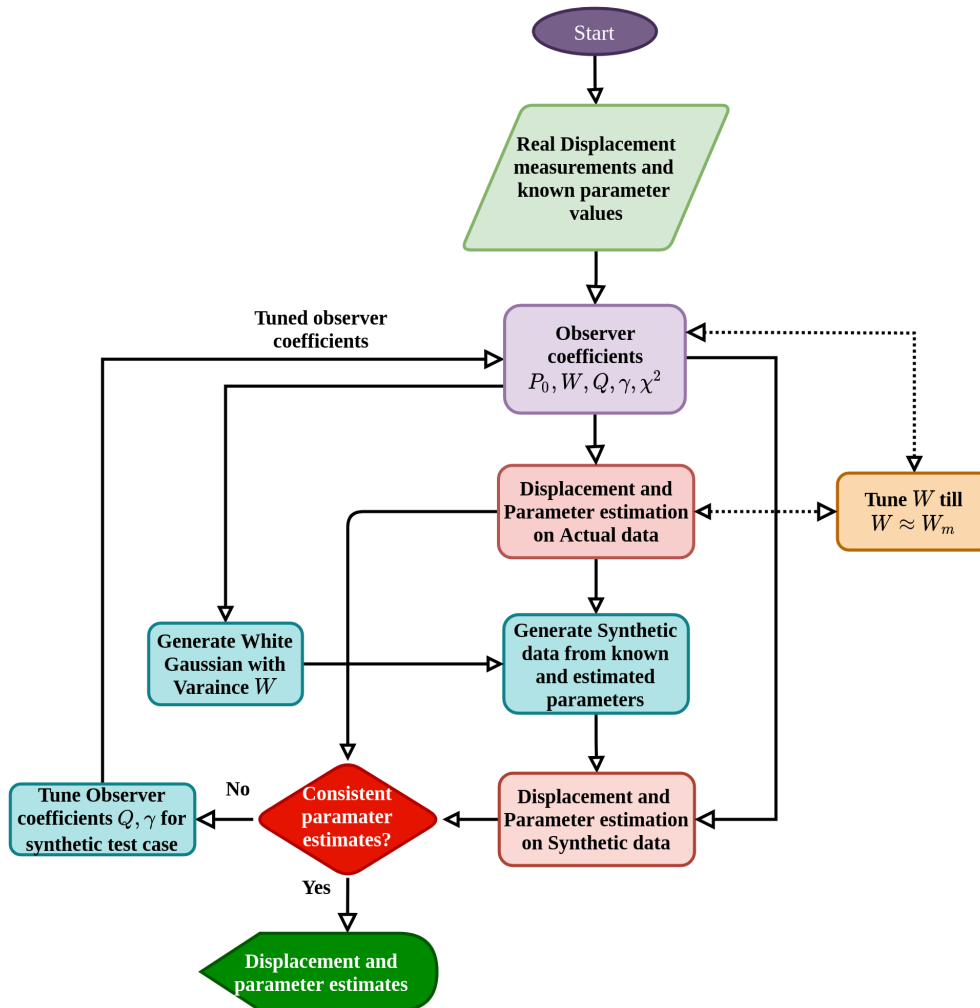


Figure 3. Observer coefficients tuning methodology

4 Estimation results

4.1 Super-Sauze landslide data

The Super-Sauze landslide is a slow-moving earthflow located in the southern French Alps which is monitored by the French Multidisciplinary Observatory OMIV for meteorological parameters, slope hydrology and slope kinematics. Detailed descriptions of this landslide and of the monitoring system can be found in previous studies (Bernardie et al., 2014; Travelletti and Malet, 2012; Malet et al., 2005). It should be mentioned that the landslide, whose volume is estimated around 560 000 m³, is characterized by a spatially heterogeneous displacement pattern with average velocities varying between 0.001 and 0.03 m.day⁻¹ (Bernardie et al., 2014). Clearly, the simple slide block model used in this study cannot aim to reproduce this

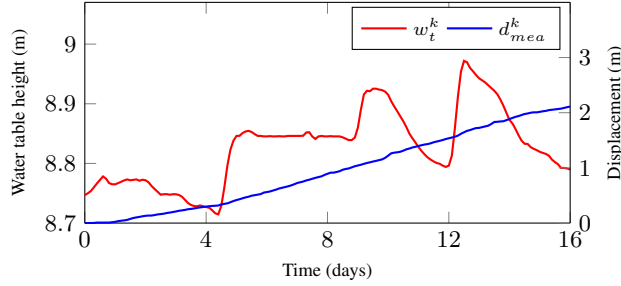


Figure 4. Super-Sauze landslide data from 07/05/1999 to 23/05/1999: Displacement measurement d_{mea}^k and reconstructed water table height time-series w_t^k obtained from Bernardie et al. (2014) (notice that w_t^k is referenced to the base of the sliding block, thus $w_t^k \leq 9$ m)

complex process. However, in line with model assumptions, displacements are mainly parallel to the dip direction of slope.
 205 The landslide is characterized by two vertical units, with a slip surface in between. Velocities appear to be mainly controlled by evolutions of the water table level, with accelerations up to $0.4 \text{ m}\cdot\text{day}^{-1}$ typically observed during spring. We thus take advantage of the rich dataset available in this site to illustrate the proposed estimation methodology and show the robustness of the approach, focusing on one specific monitoring location.

Specifically, the observer approach is applied to displacement d_{mea}^k and pore water pressure p^k time-series for a period of
 210 high water table level and accelerated motion from 07/05/1999 to 23/05/1999 (16 days) (Bernardie et al., 2014). We hypothesize that the simple model considered in this study is sufficient to reproduce this acceleration phase. The data, acquired with a time resolution $dt = 2.4 \text{ h}$ (8640 s), correspond to one of the most active parts of the landslide [location B_2 in Fig. 4 of Bernardie et al. (2014)]. Displacement and pore water pressure are measured by a wire extensometer and piezometer, respectively. The piezometer is located at -4m depth, while the slip surface is at a depth of -9m . In the proposed scheme, a water table
 215 height time-series w_t^k is required as an input. Water-table height is reconstructed from pore pressure p^k using assumption of groundwater flow parallel to the slope surface (Eq. 2): $w_t^k = 5 + p^k / (\rho_w g \cos^2 \theta)$. The reconstructed water-table height time-series along with the measured displacement are shown in Fig. 4. Known parameter values are indicated in Table 1. The value of density $\rho = 1700 \text{ kg}\cdot\text{m}^{-3}$ is chosen to correspond to saturated soil density as the water table height is close to full saturation level (Fig. 4).

220 4.2 Observer results

Displacement pattern \hat{d} along with unknown soil properties $(\hat{\eta}, \hat{\phi})$ are reconstructed with the help of the proposed estimation scheme (see Section 3), for known parameter values (Table 1), displacement measurements and water table height time-series (Fig. 4). As mentioned in Section 3.5, for an assumed confidence level of 99% on measurements with a dimension equal to 1, the value of χ^2 is set to 6.635. The value of m is fixed to 5 (see Section 3.5). Initial auto-covariance of state estimation error P_0
 225 is defined as the variance of $x_0 - \hat{x}_0$, where, $x_0 = [d_0 \quad \theta_{1_0} \quad \theta_{2_0}]^T$ (generally assumed to be a diagonal matrix). Here, d_0 and

Table 1. Known geometrical and material parameter values

Parameters	Value	Unit
Initial block displacement, d_0	0	m
Slide block thickness, H	9	m
Average inclination angle, θ	25	°
Shear zone thickness, s_t	0.2	m
Acceleration due to gravity, g	9.8	m.s ⁻²
Pore water density, ρ_w	1000	kg.m ⁻³
Cohesion, C	14000	Pa
Slide block mass density, ρ	1700	kg.m ⁻³

\hat{d}_0 are equal to 0; therefore the first entry in P_0 is assumed equal to W , which represents the auto-covariance of measurement noise r . Further, since the actual values of θ_1 and θ_2 are not known, we assume initial errors of few percents of the expected values (order of magnitude), considering guesses on $\hat{\theta}_1$ and $\hat{\theta}_2$ calculated with Eq. (6) for assumed η_0 and ϕ_0 equal to 10^8 Pa.s and 35° , respectively. Finally, the matrix P_0 is thus set to

$$230 \quad P_0 = \begin{bmatrix} W & 0 & 0 \\ 0 & 10000 & 0 \\ 0 & 0 & 100 \end{bmatrix}. \quad (20)$$

For fixed observer coefficients χ^2 , m and P_0 , and starting from initial values $\gamma = 0.95$, $W = 10^{-12}$, and $Q = 10^{-12}I_{3 \times 3}$ (where $I_{3 \times 3}$ is the identity matrix of dimension 3) for the other coefficients, the estimation scheme is applied on real measurements. Based on the actual Super-Sauze data, W is manually tuned until $W \approx W_m$, where W_m is the variance of $d_{mea} - \hat{d}$. This condition gets satisfied for $W = 7.7 \times 10^{-6}$. For this set of observer coefficients ($\chi^2, m, P_0, \gamma, W, Q$), the obtained estimation
235 results are shown in Fig. 5. It is observed that the friction angle $\hat{\phi}$ is almost constant, while the viscosity $\hat{\eta}$ varies with time in correlation with water table height. Synthetic measurements are then generated based on an average value of $\hat{\phi}$ ($\hat{\phi}_{avg}$) and a filtered viscosity time-series $\hat{\eta}_{fil}$ obtained by applying a Savitzky-Golay filter on $\hat{\eta}$ (Sharifi et al., 2022; Savitzky and Golay, 1964) (Fig. 5). In the synthetically generated displacement, a random Gaussian noise with variance W is injected. Using those synthetically generated data, the estimation scheme is applied again with identical observer coefficients as in the actual case.
240 Corresponding results can be seen in Fig. 6. It is observed that the parameter estimates are not converging to $\hat{\phi}_{avg}$ and $\hat{\eta}_{fil}$ (Fig. 6(a),(b)). Therefore, the values of γ and Q are adjusted with the help of the quantitative indicator I_η (see Eq. (19)). Notice that the indicator I_η is found to be more sensitive to variations in observer coefficients than I_ϕ and I_d . This is explained by the fact that the friction angle is almost constant, while displacement is well estimated with measurement update equation (12) of the observer.

245 Based on the sensitivity analysis (Table 2), the minimum value $I_\eta = 0.4005$ is obtained for $\gamma = 0.93$ and $Q = 10^{-11}I_{3 \times 3}$. Hence, values of γ and Q in the estimation scheme are updated accordingly, and new simulation results for synthetic and actual

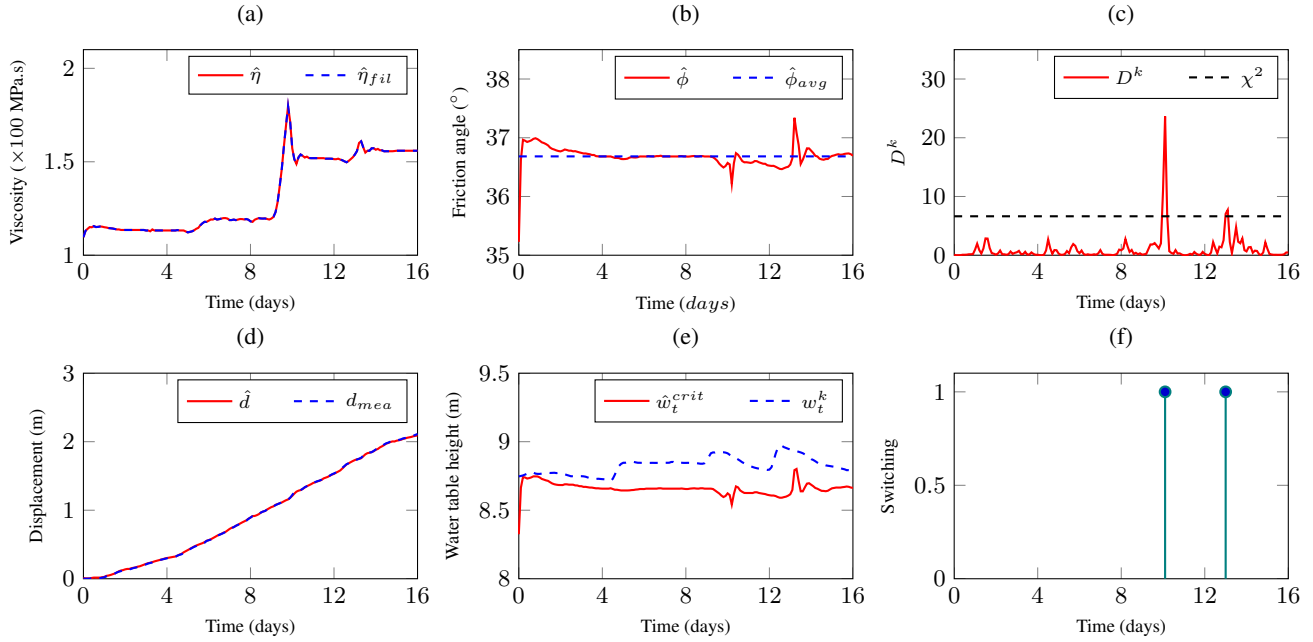


Figure 5. Initial estimation results for Super-Sauze case with *real data* and observer coefficient values $\gamma = 0.95$, $W = 7.7 \times 10^{-6}$, $Q = 10^{-12} I_{3 \times 3}$: (a)-(b) parameter estimates $(\hat{\eta}, \hat{\phi})$, filtered viscosity $\hat{\eta}_{fil}$ and averaged friction angle $\hat{\phi}_{avg}$, (c) Mahalanobis distance between estimated and measured displacement D^k , (d) displacement estimate \hat{d} and displacement measurement d_{mea} , (e) critical water table height estimate \hat{w}_t^{crit} and water table height measurement w_t^k , (f) resetting times of the covariance matrix.

Table 2. Sensitivity analysis for tuning observer coefficients γ and Q based on Super-Sauze synthetic test case: values of indicator I_η (minimum value is highlighted in bold).

γ/Q	10^{-13}	10^{-12}	10^{-11}	10^{-10}
0.95	0.7768	0.5244	0.4666	0.5628
0.96	0.7666	0.5128	0.4531	0.5534
0.93	0.7628	0.5022	0.4005	0.4501
0.92	0.7657	0.6103	0.5130	0.5567

cases are computed. Still, obtained parameter estimates are not consistent. Therefore, the process of tuning W for the actual case with condition $W \approx W_m$, and tuning γ and Q with the indicator for a synthetic test case, is continued. After 6 iterations, consistency in parameter estimates is obtained between the synthetic test case (Fig. 7 (a)-(b)) and the actual case (Fig. 8 (a)-
250 (b)). In both cases, the average value of the estimated friction angle is found to be equal to 36.8° , while approximately similar variations in estimated viscosity are observed.

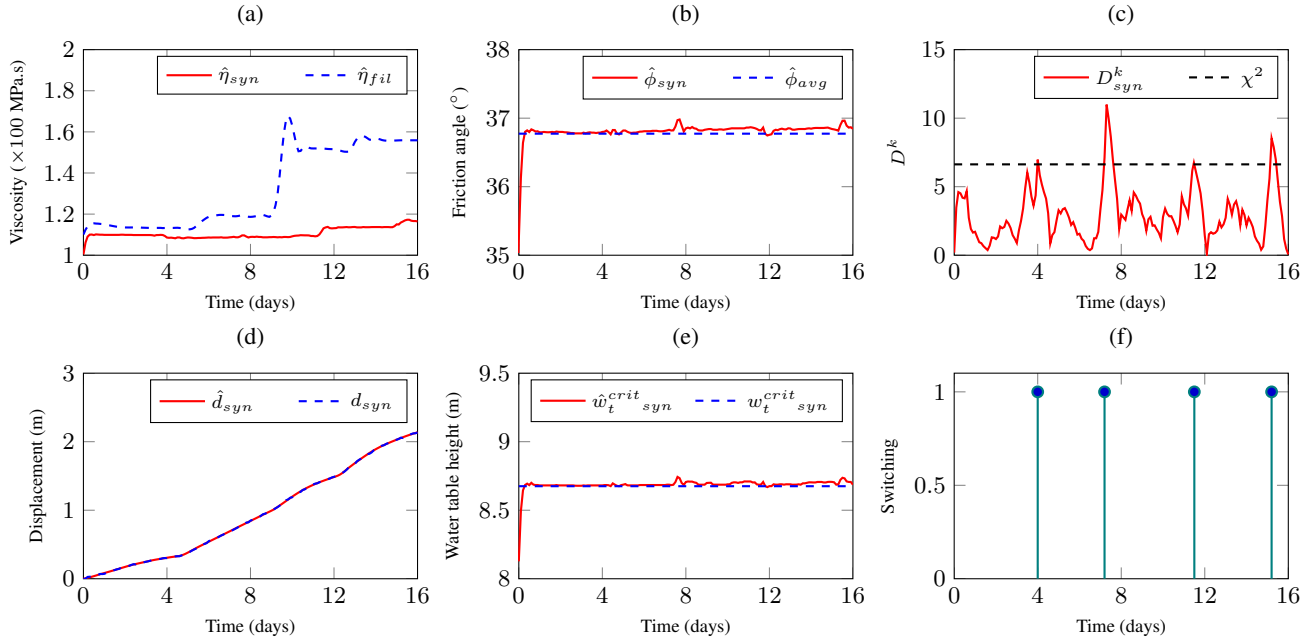


Figure 6. Initial estimation results for Super-Sauze synthetic test case with observer coefficient values $\gamma = 0.95$, $W = 7.7 \times 10^{-6}$, $Q = 10^{-12} I_{3 \times 3}$: (a)-(b) parameter estimates ($\hat{\eta}_{syn}, \hat{\phi}_{syn}$), (c) Mahalanobis distance between estimated and synthetic displacement D_{syn}^k , (d) displacement estimate \hat{d}_{syn} and synthetic displacement measurement d_{syn} , (e) critical water table height estimate $\hat{w}_t^{crit}_{syn}$, (f) resetting times of the covariance matrix.

Notice that in the final results, water-table height always remains above critical water-table height ($w_t^k > \hat{w}_t^{crit}$), as shown in Fig. 8 (e). Resetting of the covariance matrix takes place when $D^k > \chi^2$ as shown in Fig. 7 (c) and Fig. 8 (c), and the corresponding times can be seen in Fig. 7 (f) and Fig. 8 (f). Note that, as expected, these resetting times correspond to abrupt changes in viscosity.

5 Landslide displacement forecasting

The reconstruction scheme (Section 3) is based on the principle of prediction (14) followed by correction (12) of the information of interest: At each time step ' k ', information is predicted for the next time step ' $k+1$ ' with the help of Eq. (Eq. 8) and then corrected based on the measurement. This corrected information is then used to predict for the next time step, etc. In the present case, 'information' refers to displacement and parameters, i.e., $\hat{x}^k = [\hat{d}^k \quad \hat{\theta}_1^k \quad \hat{\theta}_2^k]^T$. Hence, inherently, the proposed scheme can predict information for the next time step only. However, with minor update in Eq. (14), the prediction

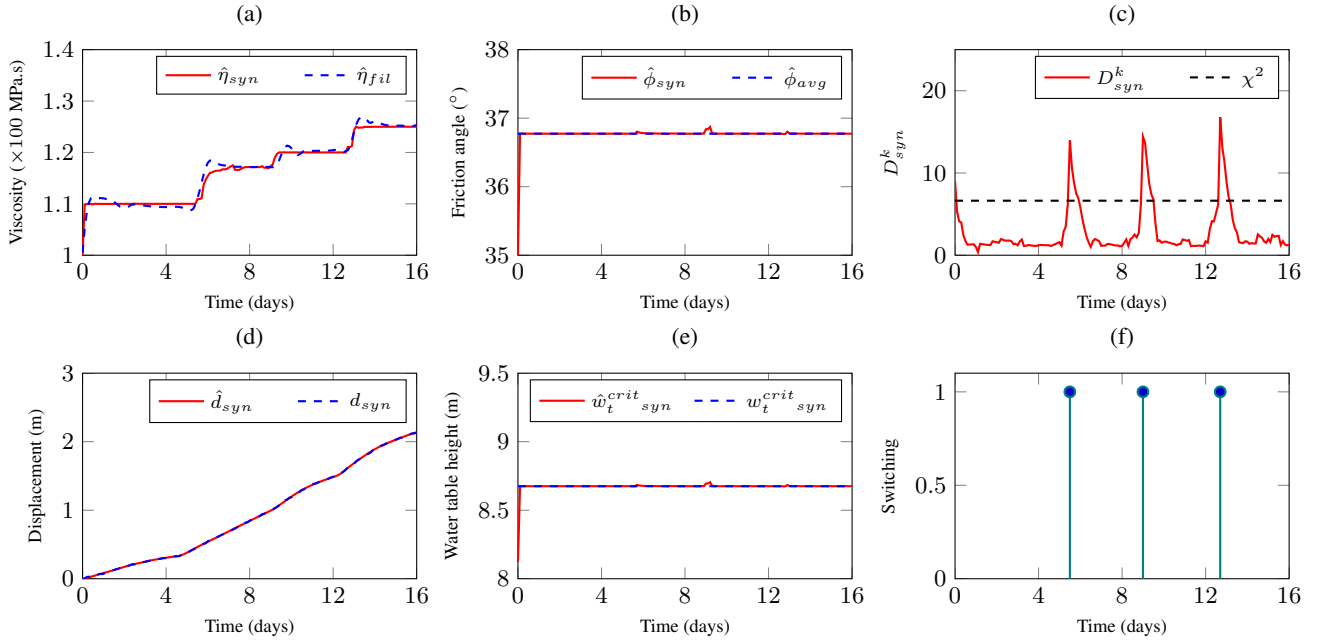


Figure 7. Final estimation results for Super-Sauze synthetic test case with observer coefficient values $\gamma = 0.9$, $W = 6 \times 10^{-5}$, $Q = 10^{-11} I_{3 \times 3}$: (a)-(b) parameter estimates ($\hat{\eta}_{syn}, \hat{\phi}_{syn}$), (c) Mahalanobis distance between estimated and synthetic displacement D_{syn}^k , (d) displacement estimate \hat{d}_{syn} and synthetic displacement measurement d_{syn} , (e) critical water table height estimate $\hat{w}_t^{crit}_{syn}$, (f) resetting times of the covariance matrix.

horizon can be extended to L time steps on the basis of the following law:

$$265 \quad \bar{x}_p^{k+l} = \begin{cases} \bar{A}^k \bar{x}_c^k & \text{for } l = 1 \\ \bar{A}^k \bar{x}_p^{k+l-1} & \text{for } l = 2 \text{ to } L - 1 \end{cases} \quad (21)$$

Notice that in order to account for the critical water table height, when a displacement value computed by (21) is lower than the former one, displacement is frozen.

To validate this extension of the approach, let us again consider the 16-day Super-Sauze landslide data. The prediction step is initiated after day eight, assuming that water table height time-series is known and that, at each time step, corresponding displacement is being measured. Two different prediction horizons are considered, namely 1 day ($L = 10$ as step size $dt =$
270 2.4 hr) and 2 days ($L = 20$). In Fig. 9 (a)-(c), displacement and parameter forecasts until day 9 and day 10 are presented. As the dynamics of time-varying parameters are a priori unknown, in model equations (7) these parameters are assumed constant, as clearly visible in Fig. 9 (b)-(c). As a consequence, it is observed that the forecast becomes rapidly less accurate as we move away from the actual time (Fig. 9 (a)). Fig. 9 (d)-(f) present moving horizon (1 day and 2 day) predictions, i.e., at instance k
275 the forecasts for $k + 10$ and $k + 20$, respectively are shown. As time advances, the estimated parameters start varying based

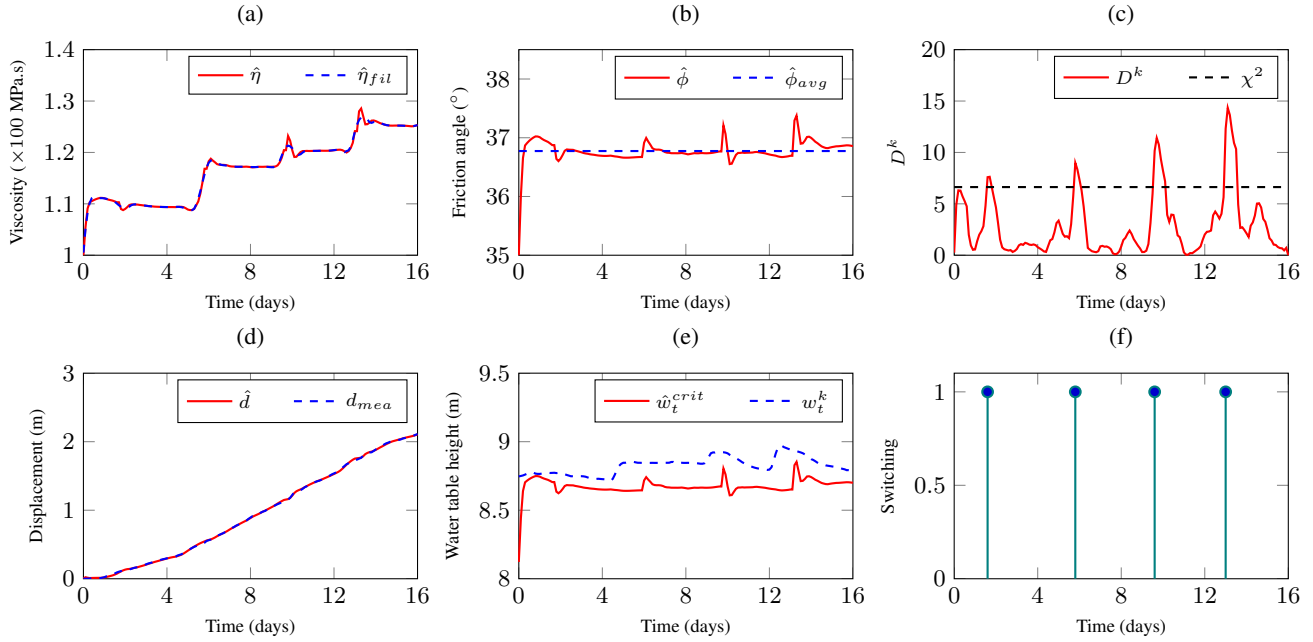


Figure 8. Final estimation results for Super-Sauze case with *real data* and observer coefficient values $\gamma = 0.9$, $W = 6 \times 10^{-5}$, $Q = 10^{-11} I_{3 \times 3}$: (a)-(b) parameter estimates $(\hat{\eta}, \hat{\phi})$, filtered viscosity η_{fil} and averaged friction angle ϕ_{avg} , (c) Mahalanobis distance between estimated and measured displacement D^k , (d) displacement estimate \hat{d} and displacement measurement d_{mea} , (e) critical water table height estimate \hat{w}_t^{crit} and water table height measurement w_t^k , (f) resetting times of the covariance matrix.

on displacement measurements and the measurement update equation of the observer (see Fig. 9 (e)-(f)). Overall, predicted displacements appear to agree reasonably well with the estimate obtained in Sec. 4. However, as it could be expected, accuracy of the forecast reduces as the prediction horizon L is increased.

6 Discussion and conclusions

280 Mechanical models capable to simulate the dynamics of landslides and predict landslide displacement over time can be of great value for the design of early warning systems. However, these models generally involve parameters (slope geometry, mechanical properties, interstitial pore pressure, etc.) that strongly influence the predictions. Among these parameters, several may be unknown and/or variable over time. In practice, the models thus need to be complemented by specific methods for parameter estimation and back-analysis. Previous studies that addressed this issue made use of relatively simple approaches, 285 such as nonlinear regression and sequential quadratic programming (Bernardie et al., 2014; Corominas et al., 2005).

In this paper, a Kalman filter methodology is proposed for the reconstruction and forecasting of landslide displacement and parameters. To illustrate the principle and capabilities of the approach, it is applied to a simplified viscoplastic sliding model

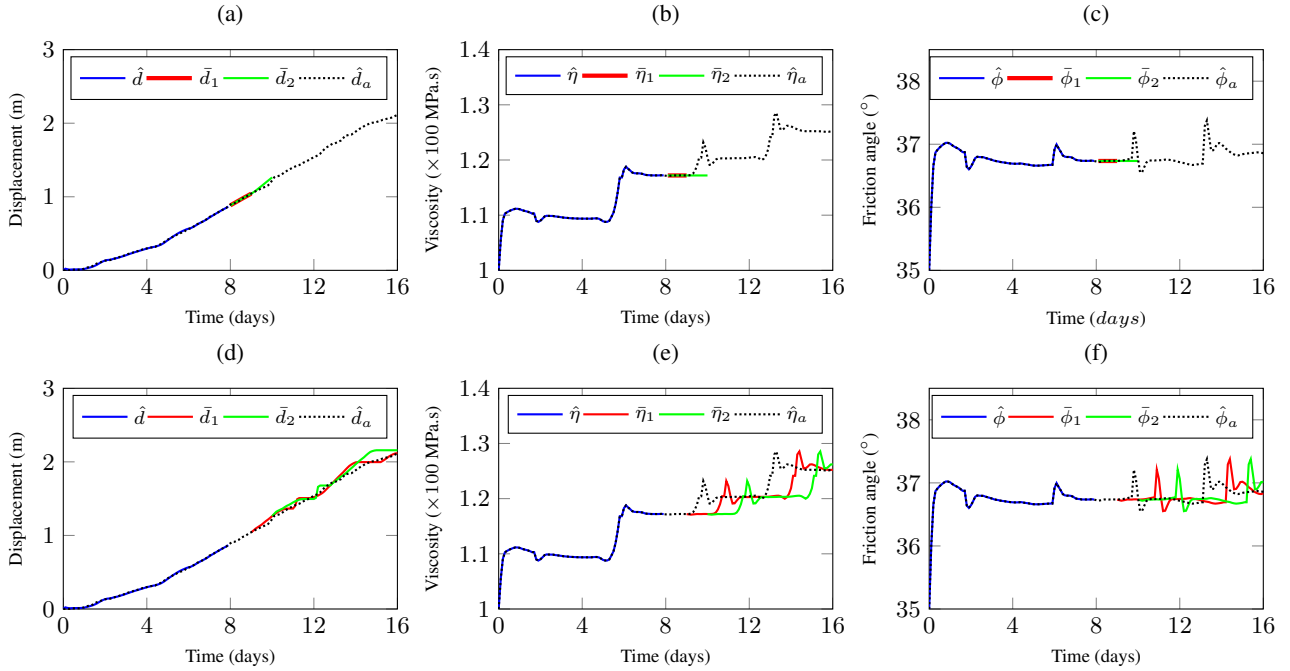


Figure 9. Landslide displacement $[\bar{d}]$ and unknown parameters $[\bar{\eta}, \bar{\phi}]$ forecasting: (a) - (c) forecasts with prediction horizon 1 day $[\bar{d}_1, \bar{\eta}_1, \bar{\phi}_1]$ and 2 days $[\bar{d}_2, \bar{\eta}_2, \bar{\phi}_2]$, (d)-(f) forecasts with moving prediction horizon 1 day $[\bar{d}_1, \bar{\eta}_1, \bar{\phi}_1]$ and 2 days $[\bar{d}_2, \bar{\eta}_2, \bar{\phi}_2]$. Plots (a) - (f) also show estimated displacement, viscosity and friction angle $[\hat{d}_a, \hat{\eta}_a, \hat{\phi}_a]$ from Section 4.

involving two unknown and possibly time-varying material parameters (friction angle ϕ and viscosity η). The reconstruction is based on displacement and water table height measurements. As the Kalman filter itself depends on several coefficients, a novel method for tuning these coefficients is proposed based on a combination of actual and synthetic test cases. The coefficients are adjusted until the estimation results obtained for both scenarios are consistent. This methodology is tested on a series of 16-days real data measured in Super-Sauze landslide (France). The results show that the friction angle ϕ was almost constant during the simulated period, while the viscosity η varied in correlation to water table height variations. Even though the reconstruction is based on a very simplified mechanical model, the obtained parameter values (namely, 36.8° for ϕ and $110 - 125$ MPa.s for η) appear to be fairly consistent with the typical ranges reported in Bernardie et al. (2014) (18 to 35° for ϕ , and 100 to 10^5 MPa.s for η). This quantitative agreement with previous studies can be seen as a validation of our approach.

The proposed scheme works on the principle of prediction followed by correction of the information of interest, i.e., at each time step, information is predicted for the next time step and then corrected based on the measurements. An approach to extend the prediction horizon over more time steps is also presented. To illustrate this extended scheme, two different prediction horizons are chosen (one day and two days). As the dynamics of time-varying parameters are unknown, they are assumed constant for the prediction horizon. As new measurements become available, the correction step takes place, and with these

corrected parameters, displacement and parameters are again predicted for the respective prediction horizon. The obtained performances are promising regarding the possibility to use such a forecast for operational predictions.

305 In summary, the results presented in this paper demonstrate that an observer-based approach coupled to a landslide mechanical model – even simple – constitutes a promising tool both for parameter estimation and displacement forecasting. We claim that this approach is highly versatile and could easily be extended to more complex mechanical models (e.g., 2D or 3D mobility models) or other types of observations (e.g., subsurface deformations), provided appropriate data are available. In this study, the application of the proposed methodology was limited to surface displacement acquired at a single location, and to a single period of time. The chosen dataset corresponds to a period of acceleration induced by high high water table levels, in line with
310 the assumptions of our model. More thorough validations over longer time periods, possibly including slow-motion phases as well as marked acceleration (fluidization) events, as in the study of Bernardie et al. (2014), will be required. In particular, the aforementioned reference showed that growing discrepancies between predicted and observed displacements during sudden fluidization events might be used to define alert thresholds. Investigating whether similar thresholds can be derived from our model represents an interesting prospect. Such developments might however require improving the model to better account for
315 the rheology of the material in a wide range of slip rates. Let us also recall that water table height variations for the prediction horizon were assumed to be known in the present study. Extending the model to estimate water table height variations from precipitation forecasts through statistical or physically-based approaches shall also be considered.

. M. Mishra was involved in the main investigation task, under joint supervision of G. Besançon, G. Chambon and L. Baillet. All authors contributed to the conceptualization, while M. Mishra more particularly developed the related code and handled the data. He also initiated
320 the writing of the original draft, to which all other authors then contributed as well. G. Besançon and G. Chambon paid a special attention to the methodology, and L. Baillet helped in the validation.

. The authors declare that they have no conflict of interest to disclose.

. This work has been supported by the French National Research Agency in the framework of the Investissements d'Avenir program (ANR-15-IDEX-02) and the Cross-Disciplinary project RISK@UGA.

325 References

- Acar, M., Ozludemir, M. T., Erol, S., Celik, R. N., and Ayan, T.: Kinematic landslide monitoring with Kalman filtering, *Natural Hazards and Earth System Sciences*, 8, 213–221, <https://doi.org/10.5194/nhess-8-213-2008>, 2008.
- Ali, A., Huang, J., Lyamin, A., Sloan, S., Griffiths, D., Cassidy, M., and Li, J. L.: Simplified quantitative risk assessment of rainfall-induced landslides modelled by infinite slopes, *Engineering Geology*, 179, <https://doi.org/10.1016/j.enggeo.2014.06.024>, 2014.
- 330 Alvioli, M., Guzzetti, F., and Rossi, M.: Scaling Properties of Rainfall-Induced Landslides Predicted by a Physically Based Model, *Geomorphology*, 213, 38, <https://doi.org/10.1016/j.geomorph.2013.12.039>, 2014.
- Anderson, B. and Moore, J.: *Optimal Filtering*, Prentice-Hall, 1979.
- Angeli, M., Buma, J., Gasparetto, P., and Pasuto, A.: A combined hillslope hydrology/stability model for low-gradient clay slopes in the Italian Dolomites, *Engineering Geology*, 49, 1–13, [https://doi.org/10.1016/S0013-7952\(97\)00033-1](https://doi.org/10.1016/S0013-7952(97)00033-1), 1998.
- 335 Angeli, M.-G., Pasuto, A., and Silvano, S.: A critical review of landslide monitoring experiences, *Engineering Geology*, 55, 133–147, [https://doi.org/10.1016/S0013-7952\(99\)00122-2](https://doi.org/10.1016/S0013-7952(99)00122-2), 2000.
- Asch, T. and Genuchten, P.: A comparison between theoretical and measured creep profiles of landslides, *Geomorphology*, 3, 45–55, [https://doi.org/10.1016/0169-555X\(90\)90031-K](https://doi.org/10.1016/0169-555X(90)90031-K), 1990.
- Bernardie, S., Desramaut, N., Malet, J., Maxime, G., and Grandjean, G.: Prediction of changes in landslide rates induced by rainfall, *Landslides*, 12, <https://doi.org/10.1007/s10346-014-0495-8>, 2014.
- 340 Bottelin, P., Baillet, L., Larose, E., Jongmans, D., Hantz, D., Brenguier, O., Cadet, H., and Helmstetter, A.: Monitoring rock reinforcement works with ambient vibrations: La Bourne case study (Vercors, France), *Engineering Geology*, 226, 136–145, <https://doi.org/10.1016/j.enggeo.2017.06.002>, 2017.
- Breton, M. L., Baillet, L., Larose, E., Rey, E., Benech, P., Jongmans, D., Guyoton, F., and Jaboyedoff, M.: Passive radio-frequency identification ranging, a dense and weather-robust technique for landslide displacement monitoring, *Engineering Geology*, 250, 1–10, <https://doi.org/10.1016/j.enggeo.2018.12.027>, 2019.
- 345 Bui, D. T., Tsangaratos, P., Nguyen, V.-T., Liem, N. V., and Trinh, P. T.: Comparing the prediction performance of a Deep Learning Neural Network model with conventional machine learning models in landslide susceptibility assessment, *CATENA*, 188, 104426, <https://doi.org/10.1016/j.catena.2019.104426>, 2020.
- 350 Caine, N.: The Rainfall Intensity: Duration Control of Shallow Landslides and Debris Flows, *Geografiska Annaler. Series A, Physical Geography*, 62, 23–27, 1980.
- Capparelli, G. and Tiranti, D.: Application of the MoniFLaIR early warning system for rainfall-induced landslides in Piedmont region (Italy), *Landslides*, 7, 401–410, <https://doi.org/https://doi.org/10.1007/s10346-009-0189-9>, 2010.
- Capparelli, G. and Versace, P.: FLAIR and SUSHI: two mathematical models for early warning of landslides induced by rainfall, *Landslides*, 355 8, 67–79, <https://doi.org/10.1007/s10346-010-0228-6>, 2011.
- Casagli, N., Intrieri, E., Tofani, V., G. G., and Raspini, F.: Landslide detection, monitoring and prediction with remote-sensing techniques, *Nat Rev Earth Environ*, 4, 51–64, 2023.
- Chae, B.-G., Park, H.-J., Catani, F., Simoni, A., and Berti, M.: Landslide prediction, monitoring and early warning: a concise review of state-of-the-art, *Geosciences Journal*, 21, 1033–1070, <https://doi.org/10.1007/s12303-017-0034-4>, 2017.
- 360 Corominas, J., Moya, J., Ledesma, A., Lloret, A., and Gili, J.: Prediction of ground displacements and velocities from groundwater level changes at the Vallcebre landslide (Eastern Pyrenees, Spain), *Landslides*, 2, 83–96, <https://doi.org/10.1007/s10346-005-0049-1>, 2005.

- Dikshit, A., Satyam, N., and Pradhan, B.: Estimation of Rainfall-Induced Landslides Using the TRIGRS Model, *Earth Systems and Environment*, 3, 575–584, <https://doi.org/10.1007/s41748-019-00125-w>, 2019.
- 365 Froude, M. J. and Petley, D. N.: Global fatal landslide occurrence from 2004 to 2016, *Nat. Hazards Earth Syst. Sci.*, 18, 2161–2181, <https://doi.org/10.5194/nhess-18-2161-2018>, 2018.
- Gili, J. A., Corominas, J., and Rius, J.: Using Global Positioning System techniques in landslide monitoring, *Engineering Geology*, 55, 167–192, [https://doi.org/10.1016/S0013-7952\(99\)00127-1](https://doi.org/10.1016/S0013-7952(99)00127-1), 2000.
- Gnanadesikan, R. and Kettenring, J. R.: Robust Estimates, Residuals, and Outlier Detection with Multiresponse Data, *Biometrics*, 28, 81–124, 1972.
- 370 Guzzetti, F., Peruccacci, S., Rossi, M., and Stark, C. P.: The rainfall intensity-duration control of shallow landslides and debris flows: an update, *Landslides*, 5, 3–17, 2008.
- Guzzetti, F., Gariano, S. L., Peruccacci, S., Brunetti, M. T., Marchesini, I., Rossi, M., and Melillo, M.: Geographical landslide early warning systems, *Earth-Science Reviews*, 200, 102973, 2020.
- Herrera, G., Fernandez-Merodo, J. A., Mulas, J., Pastor, M., Luzi, G., and Monserrat, O.: A landslide forecasting model using ground based SAR data: The Portalet case study, *Engineering Geology*, 105, 220–230, 2013.
- 375 Hutchinson, J. N.: A sliding-consolidation model for flow slides, *Canadian Geotechnical Journal*, 23, 115–126, 1986.
- Iverson, R. M.: Landslide triggering by rain infiltration, *Water Resour. Res.*, 36, 1897–1910, 2000.
- Kalman, R. E.: A New Approach to Linear Filtering and Prediction Problems, *Transactions of the ASME–Journal of Basic Engineering*, 82, 35–45, 1960.
- 380 Kim, M., Onda, Y., Uchida, T., and Kim, J. K.: Effects of soil depth and subsurface flow along the subsurface topography on shallow landslide predictions at the site of a small granitic hillslope, *Geomorphology*, 271, <https://doi.org/10.1016/j.geomorph.2016.07.031>, 2016.
- Kjekstad, O. and Highland, L.: Economic and social impacts of landslides, pp. 573–587, Springer Berlin Heidelberg, Berlin, Heidelberg, ISBN 978-3-540-69970-5, https://doi.org/10.1007/978-3-540-69970-5_30, 2009.
- Kumar, P., Sihag, P., Sharma, A., Pathania, A., Singh, R., Chaturvedi, P., Mali, N., Uday, K. ., and Dutt, V.: Prediction of Real-World Slope Movements via Recurrent and Non-recurrent Neural Network Algorithms: A Case Study of the Tangni Landslide, *Indian Geotech Journal*, 51, 788—810, 2021.
- 385 Larose, E., Carrière, S., Voisin, C., Bottelin, P., Baillet, L., Guéguen, P., Walter, F., Jongmans, D., Guillier, B., Garambois, S., Gimbert, F., and Massey, C.: Environmental seismology: What can we learn on earth surface processes with ambient noise?, *Journal of Applied Geophysics*, 116, 62–74, <https://doi.org/10.1016/j.jappgeo.2015.02.001>, 2015.
- 390 Larsen, M. C. and Simon, A.: A Rainfall Intensity-Duration Threshold for Landslides in a Humid-Tropical Environment, Puerto Rico, *Geografiska Annaler. Series A, Physical Geography*, 75, 13–23, 1993.
- Lu, F. and Zeng, H.: Application of Kalman Filter Model in the landslide deformation forecast, *Scientific Reports*, 10, 1028, <https://doi.org/10.1038/s41598-020-57881-3>, 2020.
- Malet, J.-P., Laigle, D., Remaître, A., and Maquaire, O.: Triggering conditions and mobility of debris flows associated to complex earthflows, *Geomorphological hazard and human impact in mountain environments*, 66, 215–235, 2005.
- 395 Mayoraz, F. and Vulliet, L.: Neural networks for slope movement prediction, *Int J Geomech*, 2 (2), 153–173, 2002.
- Mishra, M., Besançon, G., Chambon, G., and Baillet, L.: Optimal parameter estimation in a landslide motion model using the adjoint method, in: 2020 European Control Conference (ECC), pp. 226–231, <https://doi.org/10.23919/ECC51009.2020.9143819>, 2020a.

- Mishra, M., Besançon, G., Chambon, G., and Baillet, L.: Observer design for state and parameter estimation in a landslide model, *IFAC-PapersOnLine*, 53, 16 709–16 714, <https://doi.org/10.1016/j.ifacol.2020.12.1116>, 21th IFAC World Congress, 2020b.
- Pearson, K. F.: On the criterion that a given system of deviations from the probable in the case of a correlated system of variables, *The London, Edinburgh, and Dublin Philosophical Magazine and Journal of Science*, 50, 157–175, <https://doi.org/10.1080/14786440009463897>, 1900.
- Pecoraro, G., Calvello, M., and Piciullo, L.: Monitoring strategies for local landslide early warning systems, *Landslides*, 16, 213–231, 2019.
- Petley, D.: Global patterns of loss of life from landslides, *Geology*, 40, 927–930, 2012.
- 405 Pradhan, A. and Kim, Y.-T.: Application and comparison of shallow landslide susceptibility models in weathered granite soil under extreme rainfall events, *Environmental earth sciences*, <https://doi.org/10.1007/s12665-014-3829-x>, 2014.
- Pradhan, S., Vishal, V., and Singh, T., eds.: *Landslides: Theory, practice and Modelling*, *Advances in Natural and Technological Hazards Research*, vol. 50, Springer, 2019.
- Savitzky, A. and Golay, M. J.: Smoothing and differentiation of data by simplified least squares procedures., *Analytical chemistry*, 36, 1627–1639, 1964.
- 410 Sharifi, S., Hendry, M. T., Macciotta, R., and Evans, T.: Evaluation of filtering methods for use on high-frequency measurements of landslide displacements, *Natural Hazards and Earth System Sciences*, 22, 411–430, <https://doi.org/10.5194/nhess-22-411-2022>, 2022.
- Springman, S., Thielen, A., Kienzler, P., and Friedel, S.: A long-term field study for the investigation of rainfall-induced landslides, *Géotechnique*, 63, 1177–1193, <https://doi.org/10.1680/geot.11.P.142>, 2013.
- 415 Teixeira, M., Bateira, C., Marques, F., and Vieira, B.: Physically based shallow translational landslide susceptibility analysis in Tibo catchment, NW of Portugal, *Landslides*, <https://doi.org/10.1007/s10346-014-0494-9>, 2014.
- Țiclea, A. and Besançon, G.: State and parameter estimation via discrete-time exponential forgetting factor observer, in: *15th IFAC Symposium on System Identification, SYSID*, pp. 1370–1374, Saint Malo, France, ISSN 1474-6670, 2009.
- Țiclea, A. and Besançon, G.: Exponential forgetting factor observer in discrete time, *Systems & Cont. Letters*, 62, 756–763, 2013.
- 420 Travelletti, J. and Malet, J.-P.: Characterization of the 3D geometry of flow-like landslides: A methodology based on the integration of heterogeneous multi-source data, *Engineering Geology*, 128, 30–48, <https://doi.org/10.1016/j.enggeo.2011.05.003>, 2012.
- Van Asch, T., Van Beek, L., and Bogaard, T.: Problems in predicting the mobility of slow-moving landslides, *Engineering Geology*, 91, 46–55, <https://doi.org/10.1016/j.enggeo.2006.12.012>, *slope Transport Processes and Hydrology. A tribute to Jan Nieuwenhuis*, 2007.
- Westen, C.: Geo-Information tools for landslide risk assessment: an overview of recent developments, in: *9th International Symposium on*
- 425 *Landslides*, Rio de Janeiro, <https://doi.org/10.1201/b16816-6>, 2004.
- Yang, B., Yin, K., Lacasse, S., and Liu, Z.: Time series analysis and long short-term memory neural network to predict landslide displacement, *Landslides*, 16, 677–694, <https://doi.org/10.1007/s10346-018-01127-x>, 2019.
- Zuo, S., Zhao, L., Deng, D., Wang, Z., and Zhao, Z.: Reliability back analysis of landslide shear strength parameters based on a general nonlinear failure criterion, *International Journal of Rock Mechanics and Mining Sciences*, 126, 104 189, 2020.